Protein Cell 2013, 4(10): 761–770
DOI 10.1007/s13238-013-3908-x

Protein & Cell

RESEARCH ARTICLE

Crystal structures of the two membrane-proximal Ig-like domains (D3D4) of LILRB1/B2: alternative models for their involvement in peptide-HLA binding

Gol Nam[1,2,3], Yi Shi[1,4], Myongchol Ryu[1,2,3], Qihui Wang[1], Hao Song[1,2], Jun Liu[1], Jinghua Yan[1], Jianxun Qi[1], George F Gao[1,2,4]✉

[1] CAS Key Laboratory of Pathogenic Microbiology and Immunology, Institute of Microbiology, Chinese Academy of Sciences, Beijing 100101, China
[2] University of Chinese Academy of Sciences, Beijing 100049, China
[3] Institute of Microbiology, State Academy of Sciences, Pyongyang, Democratic People's Republic of Korea
[4] Research Network of Immunity and Health (RNIH), Beijing Institutes of Life Science, Chinese Academy of Sciences, Beijing 100101, China
✉ Correspondence: gaof@im.ac.cn
Received June 3 2013 Accepted July 3 2013

ABSTRACT

Leukocyte immunoglobulin-like receptors (LILRs), also called CD85s, ILTs, or LIRs, are important mediators of immune activation and tolerance that contain tandem immunoglobulin (Ig)-like folds. There are 11 (in addition to two pseudogenes) LILRs in total, two with two Ig-like domains (D1D2) and the remaining nine with four Ig-like domains (D1D2D3D4). Thus far, the structural features of the D1D2 domains of LILR proteins are well defined, but no structures for the D3D4 domains have been reported. This is a very important field to be studied as it relates to the unknown functions of the D3D4 domains, as well as their relative orientation to the D1D2 domains on the cell surface. Here, we report the crystal structures of the D3D4 domains of both LILRB1 and LILRB2. The two Ig-like domains of both LILRB1-D3D4 and LILRB2-D3D4 are arranged at an acute angle (~60°) to form a bent structure, resembling the structures of natural killer inhibitory receptors. Based on these two D3D4 domain structures and previously reported D1D2/HLA I complex structures, two alternative models of full-length (four Ig-like domains) LILR molecules bound to HLA I are proposed.

KEYWORDS LILRs, D3D4, HLA binding, crystal structure

INTRODUCTION

Initiation of the immune response and induction of immune tolerance are two key processes during infection, malignancy, and autoimmune disease, which are meticulously regulated by the balance between activating and inhibiting signaling among immune cells or molecules (Janeway and Medzhitov, 2002; Prud'homme, 2004; Kawai and Akira, 2006). As a family of regulatory immune receptors, the leukocyte immunoglobulin-like receptors (LILRs/LIRs, also called immunoglobulin-like transcripts (ILTs) or CD85s) are predominantly expressed on myeloid subsets and postulated to play a pivotal role in the regulation of immune responses and tolerance (Borges et al., 1997; Colonna et al., 1997; Cosman et al., 1997; Samaridis and Colonna, 1997; Saverino et al., 2000; Lanier, 2005). Encoded within the leukocyte receptor cluster (LRC) on human chromosome 19, LILRs are functionally related to other LRC receptors and have been reported to regulate a broad range of cells involved in the immune system (Fanger et al., 1998; Colonna et al., 2000; Dietrich et al., 2000; Saverino et al., 2000; Prod'homme et al., 2007; Morel and Bellon, 2008). For instance, LILRs on tolerogenic dendritic cells (DCs) modulate immune responses via induction of T-cell anergy and differentiation of $CD8^+$ T suppressor cells (Ts) (Kim-Schulze et al., 2006). Furthermore, LILRs exert powerful inhibitory effects on antigen-presenting cell phenotypes and subsequent T-cell

responses, and they may act to constrain the effects of Toll-like receptor signaling. LILRs also control innate immunity by either inhibiting or activating the cytotoxic activity of natural killer (NK) and natural killer T (NKT) cells via specific binding to their ligands on the target cells (Huang et al., 2009; Zheng et al., 2012).

The LILR family includes 13 distinct members, two of which are pseudogenes. The ligands for some of the LILRs have been determined to be classical and non-classical major histocompatibility complex (MHC, human leucocyte antigen (HLA) for humans) class I molecules and the class I-like molecule (Chapman et al., 1999; Shiroishi et al., 2006b). Based on the structural and biophysical characterization of binding features of LILRs to HLA molecules, a two-group classification of the family has been proposed (Willcox et al., 2003). The so-called "Group 1" receptors, which include LILRB1 (ILT2/LIR-1/CD85j), LILRB2 (ILT4/LIR-2/CD85d), LILRA1 (LIR-6/CD85i), LILRA2 (ILT1/LIR-7/CD85h), and LILRA3 (ILT6/LIR-4/CD85e), have a high conservation of MHC binding residues. In contrast, "Group 2" family members, which include LILRB3 (ILT5/LIR-3/CD85a), LILRB4 (ILT3/LIR-5/CD85k), LILRB5 (LIR-8/CD85c), LILRA4 (ILT7/CD85g), LILRA5 (ILT11/LIR-9/CD85f), and LILRA6 (ILT8/CD85b), have low conservation of such residues (Willcox et al., 2003). Within the Group 1 molecules, the complex crystal structures of the two immunoglobulin (Ig)-like domains (D1D2) of LILRB1 respectively bound to HLA-A2 and the class I-like molecule UL18, as well as the complex of LILRB2 bound to HLA-G have been determined, illuminating the interaction mode between the D1D2 domains and their HLA-related and indicating a pivotal role of D1D2 in the binding (Willcox et al., 2003; Shiroishi et al., 2006b; Yang and Bjorkman, 2008). In addition, the crystal structure of the D1 domain of LILRA3 also reveals the binding features to HLA I molecules but with reduced affinities compared to LILRB1/B2 (Ryu et al., 2011). Despite high levels of sequence similarity to LILRA3 and LILRB1/B2, the crystal structure of the extracellular D1D2 domain of LILRA2 shows structural shifts of the corresponding HLA-binding amino acids compared to LILRB1/B2, explaining its lack of binding to HLA molecules (Chen et al., 2009). In contrast, detailed analysis of the structures of the Group 2 members LILRB4 and LILRB5 indicate why they do not bind to HLA (Shiroishi et al., 2006a; Cheng et al., 2011). Regardlessly, these studies characterize the structures of the membrane-distal domains (D1 or D1D2) of LILRs and demonstrate their roles in ligand binding.

Recently, it has been reported that the inhibitory receptors LILRB1 and LILRB2 vary in their level of binding to different HLA alleles (Jones et al., 2011). The binding of LILRB2 to HLA-B*3501 and B*3503 is influenced by the polymorphic residues within the α1α2 domain of the HLA I, which is distant from the LILRB2-D1D2 binding region of the HLA I(Huang et al., 2009). Interestingly, human immunodeficiency virus (HIV)-derived peptides mutated by only one amino acid that is solvent-exposed have a substantial impact on the binding affinity of the HLA-B27 tetramer to LILRB2 (Lichterfeld et al., 2007). Furthermore, mutational escape in HLA-A11-, B8-, and B7-restricted immunodominant HIV-1 cytotoxic T lymphocyte (CTL) epitopes consistently enhances binding of the respective HLA I complexes to LILRB2 (Yang et al., 2010). One explanation for these newly identified interactive features of LILRs with HLA is that the LILR D3D4 domains may affect or even directly engage in the binding to HLA I (Lichterfeld and Yu, 2012), though the molecular basis of such an interaction has not been demonstrated.

The determination of LILR D3D4 domain structures is important for our understanding of the entire assembling mode of the four-domain LILRs on the cell surface and will highlight the molecular mechanism of the interaction of LILRs with HLA I. In consideration of the newly identified non-HLA I ligands of LILRs, such as angiopoietin-like proteins (ANGPTLs) (Zheng et al., 2012), D3D4 structures will also provide new insight into LILRs functions by elucidating the whole potential ligand binding region together with previously solved D1D2 structures (Chen et al., 2009).

Here, we report the crystal structures of the D3D4 domains of both LILRB1 and LILRB2, the first solved D3D4 domain structures in the LILRs family. Different from the previously determined D1D2 domains of LILRs, an uncommon architecture of the two membrane-proximal domains was observed, which is similar to the domain arrangement in KIR2DL3 (Maenaka et al., 1999). Based on detailed structural analyses of the D3D4 domains of LILRs and the previous HLA I/D1D2 complexes, two alternate models of the entire ecto-domain of LILRs complexed with HLA I are proposed.

RESULTS

Overall structures of the D3D4 domains

Both LILRB1-D3D4 and LILRB2-D3D4 are comprised of two Ig-like domains as expected, with each composed of β-strands arranged into two anti-parallel β-sheets. The topology of the LILRB1-D3D4 and LILRB2-D3D4 domains is similar to that of the LILRB1-D1D2 and LILRB2-D1D2 domains but with some distinctive features (Fig. 1). Both the LILRB1-D3 and LILRB2-D3 domains contain β-strands arranged into two anti-parallel β-sheets, with one β-sheet containing three anti-parallel β-strands (A, B, and E) and the second containing four anti-parallel β-strands (C', C, F, and G). In the D3 domain, two poly-proline II helices are located in the A-B and F-G loops, and one 3_{10} helix is located in the E-F loop.

However, the topology of the D4 domain differs between LILRB1 and LILRB2. The LILRB1-D4 domain is comprised of β-strands arranged into two anti-parallel β-sheets, with one β-sheet containing five anti-parallel β-strands (A, B, B′, E, and E′) and the second containing three anti-parallel β-strands (C′, C, and F). The G strand is disordered in the LILRB1-D3 domain structure. The LILRB2-D4 domain is composed of β-strands arranged into two anti-parallel β-sheets, with one β-sheet containing four anti-parallel β-strands (A, B, E, and C″) and the second containing four anti-parallel β-strands (C′, C, F,

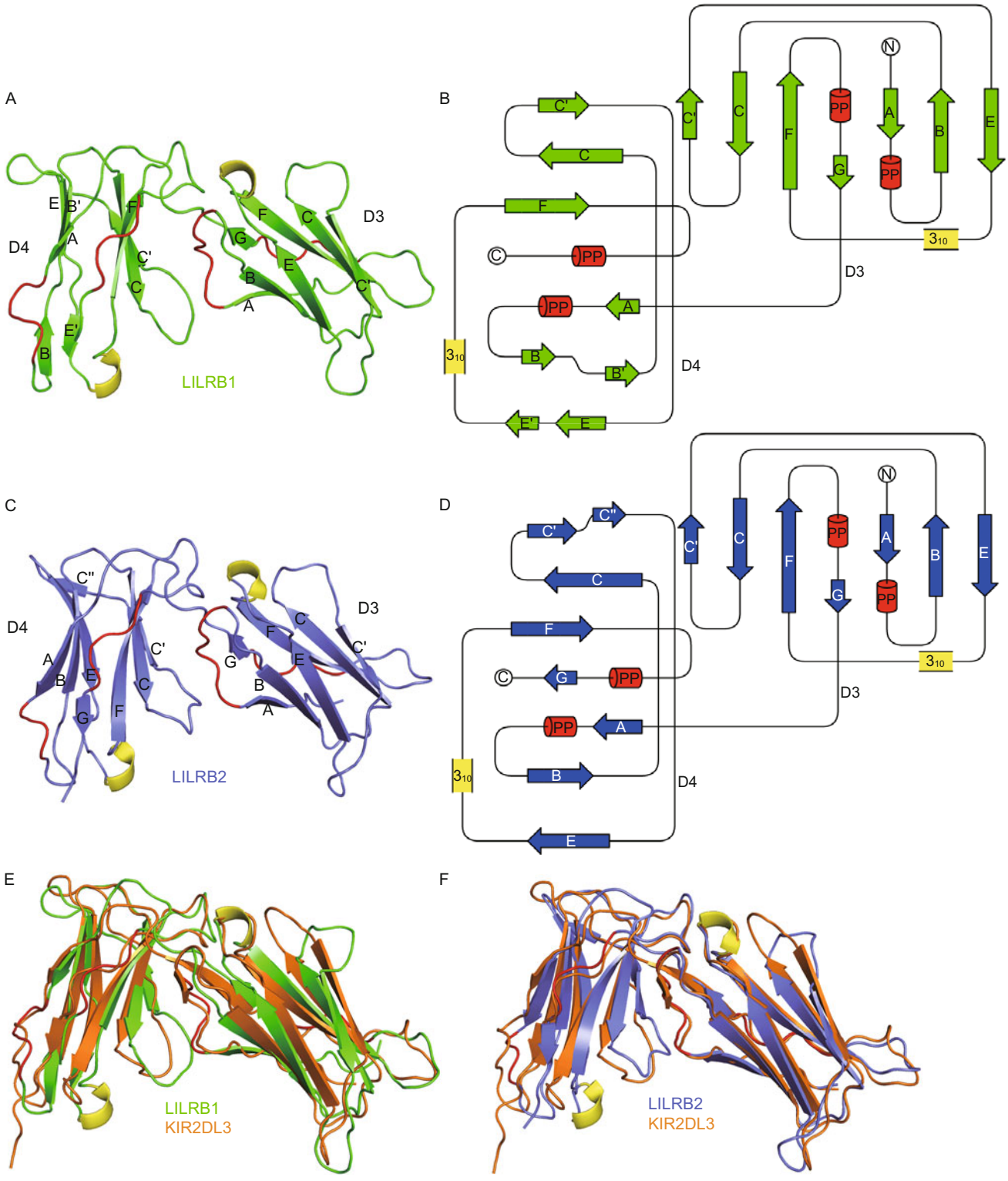

Figure 1. Overall structures of the D3D4 domains of LILRB1 and LILRB2. (A) Ribbon diagram of the LILRB1-D3D4 structures, with 3_{10} helices indicated in yellow and polyproline II helices shown in red. (B) Topological diagram of the LILRB1-D3D4 structure. (C) Ribbon diagram of the LILRB2-D3D4 structure, with 3_{10} helices indicated in yellow and polyproline II helices shown in red. (D) Topological diagram of the LILRB1-D3D4 structure. (E and F) Stereoview of LILRB1 (green) and LILRB2 (blue) D3D4 domains superimposed on KIR2DL3 (orange) through Cα atoms.

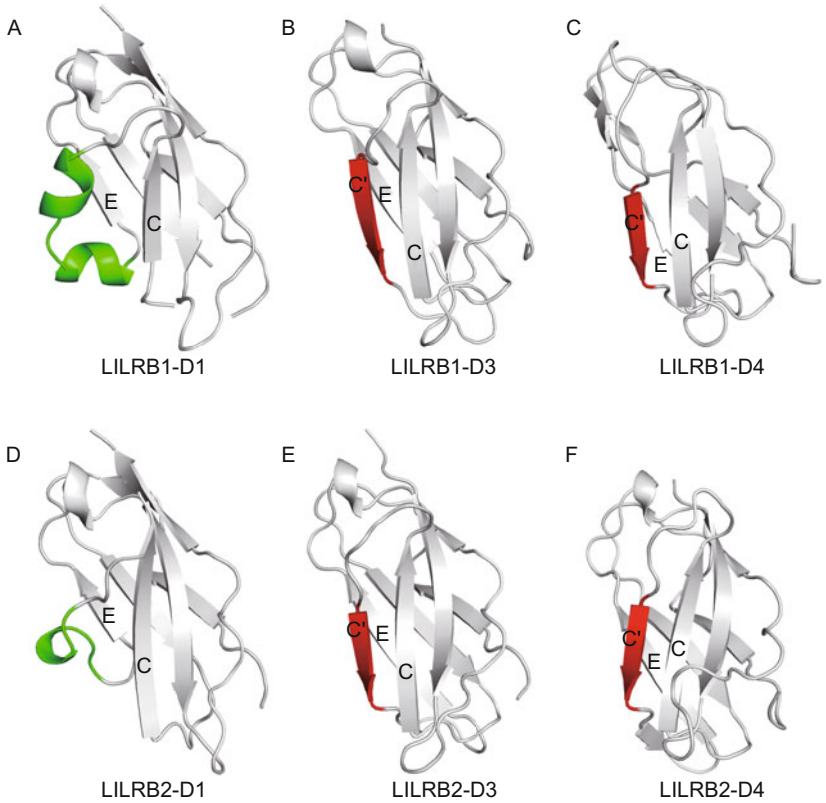

Figure 2. Comparison of secondary structural elements in the C-C′ region of LILRB1-D1 (A), LILRB1-D3 (B), LILRB1-D4 (C), LILRB2-D1 (D), LILRB2-D3 (E), and LILRB2-D4 (F). Helical elements in the C-C′ region are shown in green and β-strands in red. β-strands are observed in the C-C′ regions of LILRB1-D3, LILRB1-D4, LILRB2-D3, and LILRB2-D4, compared to 3_{10} helices in the same regions of LILRB1-D1 and LILRB2-D1.

and G). Similar to the D3 domain, two polyproline II helices are located in the A-B and F-G loops, and one 3_{10} helix is located in the E-F loop.

A Dali search (http://ekhidna.biocenter.helsinki.fi/dali_server) identified several similar structures to LILRB1-D3D4 and LILRB2-D3D4, including KIR2DL3 (PDB accession 1B6U, Z-score 22.4, root mean square deviation (rmsd) 2.5 Å for 190 amino acids), KIR2DS4 (PDB accession 3H8N, Z-score 22.2, rmsd 3.0 Å for 189 amino acids), and KIR2DL2 (PDB accession 2DLI, Z-score 21.8, rmsd 2.6 Å for 189 amino acids). This implies that the D3D4 domains may function similarly to the KIR molecules.

Comparison with LILR D1D2 domain structures

The topology of the LILRB1/B2-D1 domains includes β-strands arranged into two anti-parallel β-sheets, with one β-sheet containing three anti-parallel β-strands (A, B, and E) and the second containing four anti-parallel β-strands (C, F, G, and A′) and a 3_{10} helix (Chapman et al., 2000; Willcox et al., 2002). Compared to LILRB1/B2-D1 domains, the LILRB1/B2-D3 and -D4 domains have two main structural differences. First, the 3_{10} helix between the C and E strands is replaced by a C′ strand. Second, the A′ strand is replaced by a polyproline II helix (Figs. 1 and 2).

Interestingly, previous studies demonstrate that the 3_{10} helix region between the C and E strands in LILRB2-D1 is directly involved in the recognition of the α3 domain of HLA-G (Shiroishi et al., 2006b), and the corresponding region of LILRB1-D1 is also involved in interactions with the α3 domain of HLA-A2 (Willcox et al., 2003). Alterations in this region of LILRB1/B2-D3 and LILRB1/B2-D4 could affect binding to HLA molecules. Notably, the C′ strand we observe in the LILRB1/B2-D3 and LILRB1/B2-D4 structures has previously been noted in LILRA2-D1, LILRA5-D1, and LILRB4-D1 (Shiroishi et al., 2006a; Chen et al., 2009; Cheng et al., 2011), suggesting that the LILRB1/B2-D3D4 domains might bind similar ligands to LILRA2, LILRA5, or LILRB4. In contrast, the 3_{10} helix observed between the E and F strands in LILRB1/B2/A5-D1 is preserved in the LILRB1/B2-D3 domain. Additionally, the new polyproline II helix between the A and B strands in the LILRB1/B2-D3 domains, which is close to the inter-domain region, implicates that the inter-domain interaction between D3 and D4 might be different from that between the D1 and D2 domains.

The LILRB1/B2-D4 domains also display a new 3_{10} helix between the E and F strands, which does not exist in the D2 domains of most LILRs, with the exception of the LILRB4 receptor. This feature further confirms our previous conclusion

that the LILRB4-D2 domain is most closely related to the D4 domains of other LILRs (Cheng et al., 2011). LILRB4-D2 also displays another novel 3_{10} helix between the C and C′ strands, but this helical region does not exist in the LILRB1/B2-D4 domains.

Hinge region angles of the D3D4 domains

Previous studies indicate that the inter-domain interface of LILRs is stabilized by both inter-domain hydrogen bonds and hydrophobic interactions that are relatively conserved across the family (Chapman et al., 2000; Willcox et al., 2002; Shiroishi et al., 2006a; Cheng et al., 2011). In previous LILR structures, the D1-D2 hinge region angles are ~90° in their ligand-free forms, except that the D1-D2 hinge region angle of LILRB4 is 107° in its ligand-free form (Fig. 3) (Note: as discussed above, LILRB4 is unique). Strikingly, the D3-D4 hinge region angles of LILRB1/B2 are ~60° in their ligand-free forms (Fig. 3). This much smaller hinge region angle results from distinct feature of the D3-D4 domain interface.

For the LILRB1/B2-D1D2 domains, a conserved hydrophobic inter-domain contact region (hydrophobic core) is formed by D1 residues (V15, V94, and T96) and D2 residues (Y175 and W185), especially the W185 located in the center of the contact region, contributing to the size of the hydrophobic core, with an open shape (Fig. 4). In addition to the key hydrophobic core, other D1 residues (W67, A70, and R72 for LILRB1 and W67, T70, and R72 for LILRB2) and D2 residues (Y183 and E184 for LILRB1 and Y183 and V184 for LILRB2) are also involved in the inter-domain interaction.

For the LILRB1/B2-D3D4 domains, a similar hydrophobic core is formed by D3 residues (I15, L97, and A99 for LILRB1 and V15, L97, and T99 for LILRB2) and D4 residues (Y178 and L188) (Fig. 4). The less bulky L188 is located in the center of the contact region, contributing less to the size of the hydrophobic core, with a converged shape. In addition to the hydrophobic core, other D3 residues (R69, G72, and Q74) and D4 residues (Y186 and L187) are involved in the inter-domain interaction as well. The less bulky D3 residues further contribute to a smaller hinge region angle between the D3-D4 domains.

Interestingly, in LILRB4, the inter-domain hydrophobic core is formed by D1 residues (V15, V93, and T95) and D2 residues (F173 and L183; H139, P140, L141, and L142 from the C-C′ 3_{10} helix) (Cheng et al., 2011). The same less bulky L183 is in the center of the contact region, but LILRB4 displays a larger hinge region angle (107°). This larger angle is most likely due to the unique LILRB4-D2 C-C′ 3_{10} helix, which enlarges the size of the hydrophobic core, with a more open shape. Thus, the less bulky leucine residue could make the hinge region of the two Ig domains more flexible than the aromatic residue tryptophan.

Alternative models of HLA binding to the LILR ectodomain

Previous structural investigations of LILR-HLA I complex structures are restricted to the two most distal extracellular

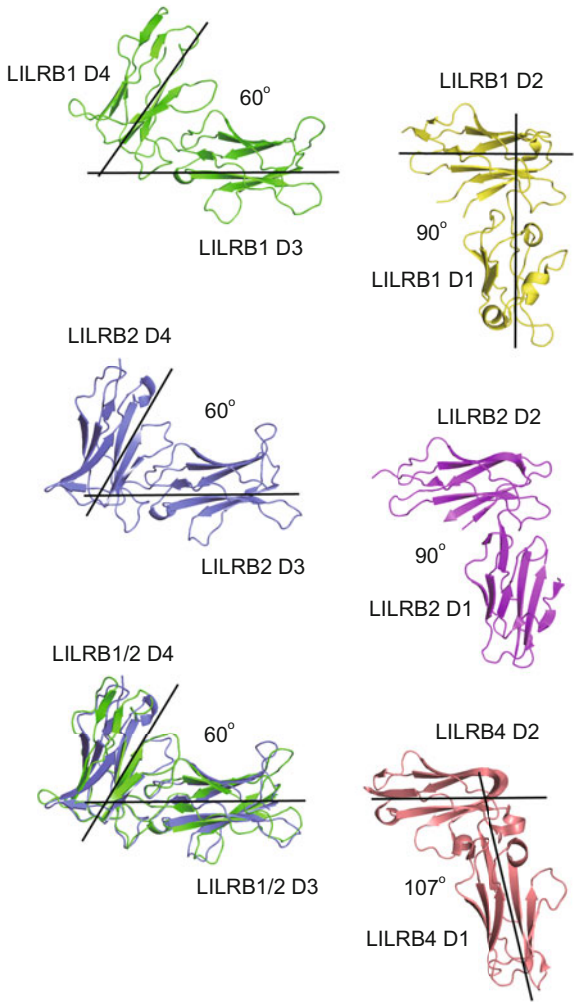

Figure 3. Comparison of the inter-domain angles of LILRB1-D3D4 and LILRB2-D3D4 with LILRB1-D1D2, LILRB2-D1D2, and LILRB4-D1D2. Both LILRB1-D3D4 and LILRB2-D3D4 show a more acute angle than LILRB1-D1D2, LILRB2-D1D2, and LILRB4-D1D2.

domains (D1 and D2) (Willcox et al., 2003; Shiroishi et al., 2006b), which contact the α3 domain and the β2m domain of HLA class I molecules. These structural data may suggest that interactions between HLA class I alleles and LILRs are static and independent of HLA sequence polymorphisms, as most of the polymorphisms occur in the α1/α2 domain. However, increasing evidence suggests that the LILR interactions with HLA class I molecule are influenced by polymorphisms in HLA class I alleles or sequence variations in the presented antigenic peptides (Lichterfeld et al., 2007; Jones et al., 2011), especially the HLA-B*35 Px subtypes accelerating HIV-1 disease progression by increasing the LILRB2-dependent but not LILRB1-dependent functional inhibition of DCs (Huang et al., 2009).

Based on our crystal structures of the LILRB1-D3D4 and LILRB2-D3D4 domains, as well as previously reported LILRB1-D1D2/HLA-A2 and LILRB2-D1D2/HLA-G complex structures,

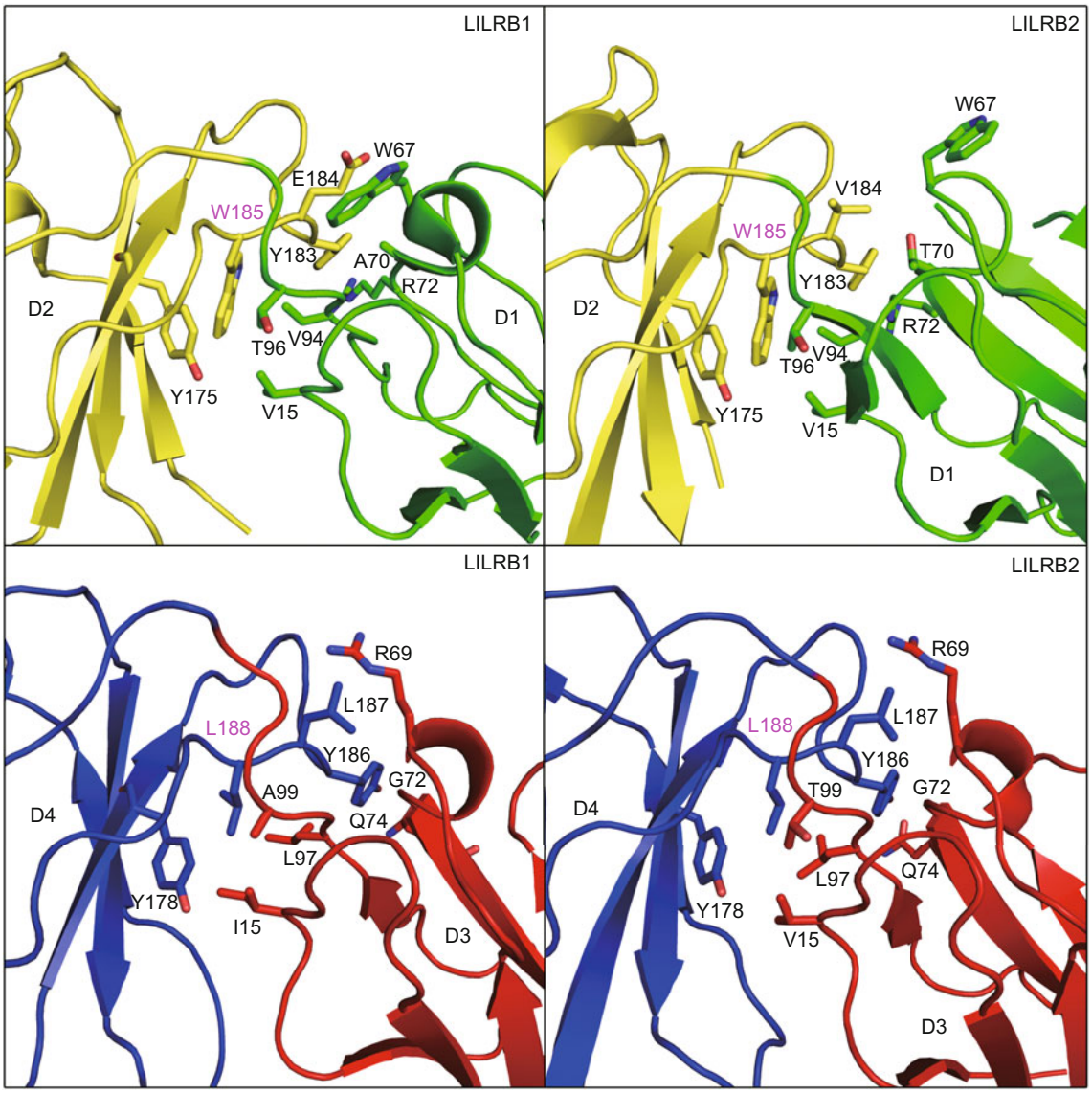

Figure 4. Structural features at the interfaces between the D1 and D2 or D3 and D4 domains of LILRB1 and LILRB2. Critical differences between the D1-D2 interface or D3-D4 interface of LILRB1 and LILRB2 are shown. For both receptors, the D1 domain is shown in green, the D2 domain in yellow, the D3 domain in red, and the D4 domain in blue. Amino acids involved in stabilizing the inter-domain interface are presented in stick representation. Both D3-D4 interfaces have less bulky residues than the D1-D2 interfaces. The residue W185 in the D1-D2 interface contributes a great deal to the larger inter-domain angle than that between D3 and D4, which have an equivalent relatively smaller residue L188.

we proposed two alternative models of HLA binding to the full-length LILR ectodomain (Fig. 5). The models were manually generated using Chimera software. The main difference between these two models is the hinge region between the D2-D3 domains. In the first model, the LILRB1-D3D4 domains are distant from the α1/α2 domain and peptide-binding region and have no effect on the recognition of peptide variations and HLA class I allele polymorphisms. In the second model, the LILRB2-D3D4 domains are oriented toward the α1/α2 domain and peptide-binding region and are directly involved in the interaction with peptide and the α1/α2 helices. The overall interaction mode may resemble KIR binding to HLA molecules, as the D3D4 domains of LILRB1/B2 have similar three-dimensional folds to KIR molecules.

DISCUSSION

Here, we report the crystal structures of the two proximal domains (D3D4) of LILRB1 and LILRB2, the first such structures for LILR family members. The LILRB1- and LILRB2-D3D4

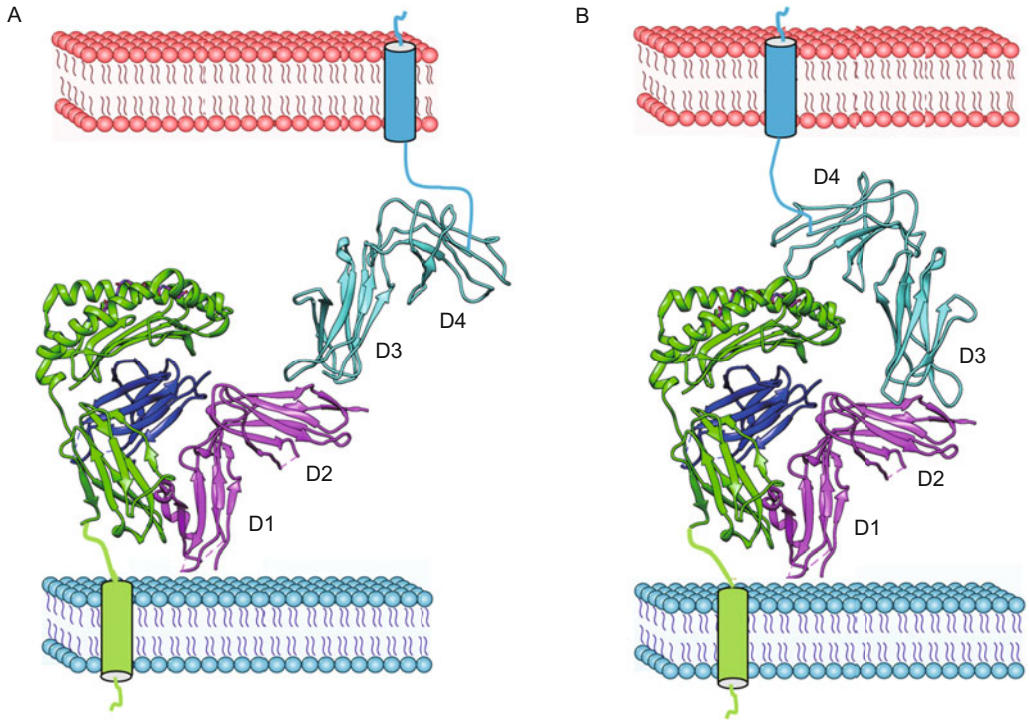

Figure 5. Alternative models of full-length LILR molecules binding to peptide-HLA (pHLA). (A) Model of full-length LILRB1 binding to pHLA. The model was generated by combining the LILRB1-D1D2/HLA-A2 complex structure with the LILRB1-D3D4 structure. The orientation between the D2 and D3 domains was manually linked to orient the D3D4 domains away from the pHLA. (B) Model of full-length LILRB2 binding to pHLA. The model was generated by combining the LILRB2-D1D2 and HLA-G complex structure with the LILRB2-D3D4 structure. The orientation between the D2 and D3 domains was manually linked to orient the D3D4 domains toward the pHLA.

domains consist of two Ig-like domains, which are similar to the LILRB1-D1D2 and LILRB2-D1D2 domains but with some distinctive features. For instance, a novel polyproline II helix was observed in the A-B loops in both the D3 and D4 domains of LILRB1 and LILRB2. The polyproline II helix of the A-B loop in the D3 domain is close to the inter-domain region and may be involved in the inter-domain interaction. Because of the high degree of identity shared between LILR family members, the LILRB1- and LILRB2-D3D4 structures can be used as a first-order model for the structures of other LILR proteins.

A Dali search identified that the structures of KIR molecules most closely resemble LILRB1-D3D4 and LILRB2-D3D4, implying that LILRB1-D3D4 and LILRB2-D3D4 may have similar functions to KIR molecules, which bind the α-helix platform of HLA I molecules. Further structural analysis revealed that the inter-domain angle (~60°) of the D3D4 domains is more acute than that (90° or 107°) of the D1D2 domains but similar to the inter-domain angle of KIR molecules. This acute inter-domain angle results from the less bulky D3 residues, which are conserved in the D3D4 domains of other LILR family members. Consistent with this, our studies of PD-L1 show that the angle between neighboring Ig domains can shift as a result of altered interactions between hydrophobic residues (Chen et al., 2010).

Previous studies demonstrate that the first two domains of LILR molecules (LILRB1 and LILRB2) mainly bind HLA I molecules through the 3_{10} helix region between the C and E strands, which is directly involved in the recognition of the α3 domain of the HLA I molecule (Willcox et al., 2003; Shiroishi et al., 2006b). However, in the D3D4 structures, the 3_{10} helix region is replaced by the C′ strand, indicating that the D3D4 domain cannot bind HLA I molecules in the same manner that D1D2 domains do, if at all.

Recent studies of the inhibitory receptors LILRB1 and LILRB2 show that they vary in their level of binding to different HLA I alleles (Jones et al., 2011). The binding of LILRB2 to HLA-B*3501 and B*3503 is influenced by the polymorphic residues within the α1α2 domain, which is distant from the LILRB2-D1D2 binding region of HLA (Huang et al., 2009). Further, HIV-derived peptides substituted by only one amino acid have a substantial impact on the binding affinity of HLA-B27 tetramers to LILRB2 (Lichterfeld et al., 2007). However, for LILRB1, no similar observations have been reported. Therefore, we propose two alternative models for full-length LILR binding to peptide-HLA molecules (Fig. 5) to interpret the differential biological outcomes of LILRB1 and LILRB2. One model shows that the D3D4 domains orient away from the α1α2 domain of the HLA molecules, while the other shows that the D3D4 domains orient toward the α1α2 domain, implicating that the D3D4 domain might be involved in the interaction with the top of the α1α2 domain via the D4 domain. These different

orientations of the D3D4 domains may be determined by different D2D3 inter-domain residues in LILRB1 and LILRB2, which requires real complex structures to confirm.

In conclusion, we provide the first glimpse into the structural features of the D3D4 domains of LILRB1 and LILRB2 and implicate how full-length LILR molecules may bind to HLA molecules. Differential orientation models of the D3D4 domains relative to D1D2 are proposed, which will promote further studies.

MATERIALS AND METHODS

Gene cloning, protein expression, and purification

The genes for the two proximal extracellular domains (D3D4; residues 230–419) of both LILRB1 and LILRB2 (LILLB1-D3D4 and LILRB2-D3D4) were cloned into the pET21a vector, respectively. The recombinant proteins were expressed in inclusion bodies in *Escherichia coli* strain BL21(DE3) pLysS (Novagen) and prepared as previously described (Chen et al., 2007). Briefly, the inclusion bodies were isolated from cell pellets by sonication and washed with washing buffer (0.5% Triton X-100, 50 mmol/L Tris-HCl, pH 8.0, 300 mmol/L NaCl, 10 mmol/L EDTA, 10 mmol/L β-mercaptoethanol (β-ME), and 0.1% NaN_3), resuspension buffer (50 mmol/L Tris-HCl, pH 8.0, 100 mmol/L NaCl, 10 mmol/L EDTA, 10 mmol/L β-ME, and 0.1% NaN_3), and then dissolved overnight in a denaturing buffer (6 mol/L guanidine hydrochloride, 50 mmol/L Tris-HCl, pH 8.0, 100 mmol/L NaCl, 10 mmol/L EDTA, 10% (*v/v*) glycerol, and 10 mmol/L DTT).

The proteins were renatured by the dilution refolding method using the following refolding buffer: 100 mmol/L Tris-HCl, 2 mmol/L EDTA, 400 mmol/L L-arginine HCl, 0.5 mmol/L oxidized glutathione, 5 mmol/L reduced glutathione, 0.1 mmol/L PMSF, and 0.1 mmol/L NaN_3, with the pH adjusted to 8.0, at a final protein concentration of 1–2 μmol/L at 4°C. The refolding reaction was incubated overnight and then concentrated using a stirred cell and ultra-centrifugal filter devices (Millipore). Refolded protein was purified by size exclusion chromatography using a HiLoad™ Superdex® 75 16/60 PG column with an AKTA FPLC (GE Healthcare). LILRB1-D3D4 and LILRB2-D3D4 proteins were further purified by anion-exchange chromatography (Resource Q, GE Healthcare).

Crystallization and data collection

Both purified LILRB1-D3D4 and LILRB2-D3D4 were concentrated to 20 mg/mL in a buffer consisting of 20 mmol/L Tris, pH 8.0, and 50 mmol/L NaCl. Initial screening of crystallization conditions was performed using sparse matrix approaches with commercial screening kits supplied by Hampton Research. All crystallization experiments were performed using the vapor diffusion method at both 18°C and 4°C. Rod-shaped crystals of LILRB1-D3D4 were obtained in hanging drops equilibrated against a reservoir solution containing 0.2 mol/L NaI, pH 6.9, and 10 mg/mL protein at 4°C. Crystals of LILRB2-D3D4 were obtained in hanging drops with a reservoir solution containing 3.5 mol/L sodium formate, 0.1 mol/L Tris, pH 8.0, and 10 mg/mL protein at 18°C. For data collection, crystals were soaked in reservoir buffer supplemented with 15% (*v/v*) glycerol for 60 s before they were flash-cooled to 100 K in a nitrogen gas stream. X-ray diffraction data were collected at the Shanghai Synchrotron Radiation Facility (SSRF) beamline 17U (Table 1). All data were processed with HKL2000 (Otwinowski and Minor, 1997).

The LILRB1-D3D4 structure was solved by single wavelength anomalous dispersion (SAD) using 2.7 Å data from a crystal soaked with iodine. The crystal structure of the D3D4 domains of LILRB2 was solved to 2.5 Å by molecular replacement using Phaser (Read, 2001) from the CCP4 program suite (Collaborative Computational Project, 1994) and the crystal structure of LILRB1-D3D4 as a search model. Initial rigid body refinement was performed using REFMAC5 (Murshudov et al., 1997), and extensive model building was performed using COOT (Emsley and Cowtan, 2004). Further rounds of refinement were performed using the phenix.refine program implemented in the PHENIX package (Adams et al., 2010) with energy minimization, isotropic ADP refinement, and bulk solvent modeling. The structures were then adjusted using COOT and refined with PHENIX. Final statistics for data collection and structure refinement are represented in Table 1. The stereochemical quality of the final model was assessed with the program PROCHECK (Laskowski et al., 1993).

Table 1. Statistics for crystallographic data collection and structure refinement

	LILARB1-D3D4	LILRB2-D3D4
Data collection		
Space group	C2	P21
Cell dimensions		
a, *b*, *c* (Å)	121.26 71.98 75.04	57.37 66.17 83.72
α, β, γ (°)	90, 95, 90	90, 95, 90
Resolution (Å)	50.0–2.7	50.0–2.5
R_{merge}	0.087 (0.524)	0.082 (0.597)
$I/\sigma I$	15.5 (2.7)	16.4 (2.2)
Completeness (%)	97.5 (96.5)	99.7 (99.5)
Redundancy	3.7 (3.7)	3.7 (3.7)
Refinement		
Resolution (Å)	32.8–2.7	43.2–2.5
No. reflections	16729	21645
R_{work}/R_{free}	0.2432/0.2886	0.2213/0.2717
No. atoms		
Protein	4497	4539
Water	90	71
B-factors		
Protein	68.3	51.8
Water	49.1	38.8
R.m.s. deviations		
Bond lengths (Å)	0.011	0.007
Bond angles (°)	1.693	1.311
Ramachandran Plot (%)		
Most favoured regions	77.9	91.7
Additional allowed regions	20.6	7.9
Generously allowed regions	1.5	0.4
Disallowed regions	0	0

*Values in parentheses are for highest-resolution shells.

PROTEIN DATA BANK ACCESSION NUMBERS

The atomic coordinates of LILRB1-D3D4 and LILRB2-D3D4 have been deposited in the RCSB Protein Data Bank with accession codes 4LL9 and 4LLA, respectively.

ACKNOWLEDGEMENTS

We thank the staff at the Shanghai Synchrotron Radiation Facility (SSRF-beamline 17U) for crystal data collection.

This work was supported by the China National Grand S&T Special Project (No. 2012ZX10001006) and the National Natural Science Foundation of China (Grant No. 31030030). GFG is a leading principal investigator of the NSFC Innovative Research Group (Grant No. 81021003).

COMPLIANCE WITH ETHICS GUIDELINES

Gol Nam, Yi Shi, Myongchol Ryu, Qihui Wang, Hao Song, Jun Liu, Jinghua Yan, Jianxun Qi and George F Gao declare that they have no conflict of interest.

This article does not contain any studies with human or animal subjects performed by the any of authors.

REFERENCES

Adams, P.D., Afonine, P.V., Bunkoczi, G., Chen, V.B., Davis, I.W., Echols, N., Headd, J.J., Hung, L.W., Kapral, G.J., Grosse-Kunstleve, R.W., et al. (2010). PHENIX: a comprehensive Python-based system for macromolecular structure solution. Acta Crystallogr D Biol Crystallogr 66, 213–221.

Borges, L., Hsu, M.L., Fanger, N., Kubin, M., and Cosman, D. (1997). A family of human lymphoid and myeloid Ig-like receptors, some of which bind to MHC class I molecules. J Immunol 159, 5192–5196.

Chapman, T.L., Heikema, A.P., West, A.P., Jr., and Bjorkman, P.J. (2000). Crystal structure and ligand binding properties of the D1D2 region of the inhibitory receptor LIR-1 (ILT2). Immunity 13, 727–736.

Chapman, T.L., Heikeman, A.P., and Bjorkman, P.J. (1999). The inhibitory receptor LIR-1 uses a common binding interaction to recognize class I MHC molecules and the viral homolog UL18. Immunity 11, 603–613.

Chen, Y., Chu, F., Gao, F., Zhou, B., and Gao, G.F. (2007). Stability engineering, biophysical, and biological characterization of the myeloid activating receptor immunoglobulin-like transcript 1 (ILT1/LIR-7/LILRA2). Protein Expr Purif 56, 253–260.

Chen, Y., Gao, F., Chu, F., Peng, H., Zong, L., Liu, Y., Tien, P., and Gao, G.F. (2009). Crystal structure of myeloid cell activating receptor leukocyte Ig-like receptor A2 (LILRA2/ILT1/LIR-7) domain swapped dimer: molecular basis for its non-binding to MHC complexes. J Mol Biol 386, 841–853.

Chen, Y., Liu, P., Gao, F., Cheng, H., Qi, J., and Gao, G.F. (2010). A dimeric structure of PD-L1: functional units or evolutionary relics? Protein Cell 1, 153–160.

Cheng, H., Mohammed, F., Nam, G., Chen, Y., Qi, J., Garner, L.I., Allen, R.L., Yan, J., Willcox, B.E., and Gao, G.F. (2011). Crystal structure of leukocyte Ig-like receptor LILRB4 (ILT3/LIR-5/CD85k): a myeloid inhibitory receptor involved in immune tolerance. J Biol Chem 286, 18013–18025.

Collaborative Computational Project, N. (1994). The CCP4 suite: programs for protein crystallography. Acta Crystallogr D Biol Crystallogr 50, 760–763.

Colonna, M., Nakajima, H., and Cella, M. (2000). A family of inhibitory and activating Ig-like receptors that modulate function of lymphoid and myeloid cells. Semin Immunol 12, 121–127.

Colonna, M., Navarro, F., Bellon, T., Llano, M., Garcia, P., Samaridis, J., Angman, L., Cella, M., and Lopez Botet, M. (1997). A common inhibitory receptor for major histocompatibility complex class I molecules on human lymphoid and myelomonocytic cells [see comments]. J Exp Med 186, 1809–1818.

Cosman, D., Fanger, N., Borges, L., Kubin, M., Chin, W., Peterson, L., and Hsu, M.L. (1997). A novel immunoglobulin superfamily receptor for cellular and viral MHC class I molecules. Immunity 7, 273–282.

Dietrich, J., Nakajima, H., and Colonna, M. (2000). Human inhibitory and activating Ig-like receptors which modulate the function of myeloid cells. Microbes Infect 2, 323–329.

Emsley, P., and Cowtan, K. (2004). Coot: model-building tools for molecular graphics. Acta Crystallogr D Biol Crystallogr 60, 2126–2132.

Fanger, N.A., Cosman, D., Peterson, L., Braddy, S.C., Maliszewski, C.R., and Borges, L. (1998). The MHC class I binding proteins LIR-1 and LIR-2 inhibit Fc receptor-mediated signaling in monocytes. Euro J Immunol 28, 3423–3434.

Huang, J., Goedert, J.J., Sundberg, E.J., Cung, T.D., Burke, P.S., Martin, M.P., Preiss, L., Lifson, J., Lichterfeld, M., Carrington, M., et al. (2009). HLA-B*35-Px-mediated acceleration of HIV-1 infection by increased inhibitory immunoregulatory impulses. J Exp Med 206, 2959–2966.

Janeway, C.A., Jr., and Medzhitov, R. (2002). Innate immune recognition. Annu Rev Immunol 20, 197–216.

Jones, D.C., Kosmoliaptsis, V., Apps, R., Lapaque, N., Smith, I., Kono, A., Chang, C., Boyle, L.H., Taylor, C.J., Trowsdale, J., et al. (2011). HLA class I allelic sequence and conformation regulate leukocyte Ig-like receptor binding. J Immunol 186, 2990–2997.

Kawai, T., and Akira, S. (2006). Innate immune recognition of viral infection. Nat Immunol 7, 131–137.

Kim-Schulze, S., Scotto, L., Vlad, G., Piazza, F., Lin, H., Liu, Z., Cortesini, R., and Suciu-Foca, N. (2006). Recombinant Ig-like transcript 3-Fc modulates T cell responses via induction of Th anergy and differentiation of CD8+ T suppressor cells. J Immunol 176, 2790–2798.

Lanier, L.L. (2005). NK cell recognition. Annu Rev Immunol 23, 225–274.

Laskowski, R.A., Macarthur, M.W., Moss, D.S., and Thornton, J.M. (1993). Procheck - a Program to Check the Stereochemical Quality of Protein Structures. J Appl Crystallogr 26, 283–291.

Lichterfeld, M., Kavanagh, D.G., Williams, K.L., Moza, B., Mui, S.K., Miura, T., Sivamurthy, R., Allgaier, R., Pereyra, F., Trocha, A., et al. (2007). A viral CTL escape mutation leading to immunoglobulin-like transcript 4-mediated functional inhibition of myelomonocytic cells. J Exp Med 204, 2813–2824.

Lichterfeld, M., and Yu, X.G. (2012). The emerging role of leukocyte immunoglobulin-like receptors (LILRs) in HIV-1 infection. J Leukoc Biol 91, 27–33.

Maenaka, K., Juji, T., Stuart, D.I., and Jones, E.Y. (1999). Crystal structure of the human p58 killer cell inhibitory receptor (KIR2DL3) specific for HLA-Cw3-related MHC class I. Structure 7, 391–398.

Morel, E., and Bellon, T. (2008). HLA class I molecules regulate IFN-gamma production induced in NK cells by target cells, viral products, or immature dendritic cells through the inhibitory receptor ILT2/CD85j. J Immunol 181, 2368–2381.

Murshudov, G.N., Vagin, A.A., and Dodson, E.J. (1997). Refinement of macromolecular structures by the maximum-likelihood method. Acta Crystallogr D Biol Crystallogr 53, 240–255.

Otwinowski, Z., and Minor, W. (1997). Processing of X-ray diffraction data collected in oscillation mode. Method Enzymol 276, 307–326.

Prod'homme, V., Griffin, C., Aicheler, R.J., Wang, E.C., McSharry, B.P., Rickards, C.R., Stanton, R.J., Borysiewicz, L.K., Lopez-Botet, M., Wilkinson, G.W., et al. (2007). The human cytomegalovirus MHC class I homolog UL18 inhibits LIR-1+ but activates LIR-1- NK cells. J Immunol 178, 4473–4481.

Prud'homme, G.J. (2004). Altering immune tolerance therapeutically: the power of negative thinking. J Leukoc Biol 75, 586–599.

Read, R.J. (2001). Pushing the boundaries of molecular replacement with maximum likelihood. Acta Crystallogr D Biol Crystallogr 57, 1373–1382.

Ryu, M., Chen, Y., Qi, J., Liu, J., Fan, Z., Nam, G., Shi, Y., Cheng, H., and Gao, G.F. (2011). LILRA3 binds both classical and non-classical HLA class I molecules but with reduced affinities compared to LILRB1/LILRB2: structural evidence. PLoS One 6, e19245.

Samaridis, J., and Colonna, M. (1997). Cloning of novel immunoglobulin superfamily receptors expressed on human myeloid and lymphoid cells: structural evidence for new stimulatory and inhibitory pathways. Euro J Immunol 27, 660–665.

Saverino, D., Fabbi, M., Ghiotto, F., Merlo, A., Bruno, S., Zarcone, D., Tenca, C., Tiso, M., Santoro, G., Anastasi, G., et al. (2000). The CD85/LIR-1/ILT2 inhibitory receptor is expressed by all human T lymphocytes and down-regulates their functions. J Immunol 165, 3742–3755.

Shiroishi, M., Kajikawa, M., Kuroki, K., Ose, T., Kohda, D., and Maenaka, K. (2006a). Crystal structure of the human monocyte-activating receptor, "Group 2" leukocyte Ig-like receptor A5 (LILRA5/LIR9/ILT11). J Biol Chem 281, 19536–19544.

Shiroishi, M., Kuroki, K., Rasubala, L., Tsumoto, K., Kumagai, I., Kurimoto, E., Kato, K., Kohda, D., and Maenaka, K. (2006b). Structural basis for recognition of the nonclassical MHC molecule HLA-G by the leukocyte Ig-like receptor B2 (LILRB2/LIR2/ILT4/CD85d). Proc Natl Acad Sci U S A 103, 16412–16417.

Willcox, B.E., Thomas, L.M., and Bjorkman, P.J. (2003). Crystal structure of HLA-A2 bound to LIR-1, a host and viral major histocompatibility complex receptor. Nat Immunol 4, 913–919.

Willcox, B.E., Thomas, L.M., Chapman, T.L., Heikema, A.P., West, A.P., Jr., and Bjorkman, P.J. (2002). Crystal structure of LIR-2 (ILT4) at 1.8 A: differences from LIR-1 (ILT2) in regions implicated in the binding of the Human Cytomegalovirus class I MHC homolog UL18. BMC Struct Biol 2, 6.

Yang, Y., Huang, J., Toth, I., Lichterfeld, M., and Yu, X.G. (2010). Mutational escape in HIV-1 CTL epitopes leads to increased binding to inhibitory myelomonocytic MHC class I receptors. PLoS One 5, e15084.

Yang, Z., and Bjorkman, P.J. (2008). Structure of UL18, a peptide-binding viral MHC mimic, bound to a host inhibitory receptor. Proc Natl Acad Sci U S A 105, 10095–10100.

Zheng, J., Umikawa, M., Cui, C., Li, J., Chen, X., Zhang, C., Huynh, H., Kang, X., Silvany, R., Wan, X., et al. (2012). Inhibitory receptors bind ANGPTLs and support blood stem cells and leukaemia development. Nature 485, 656–660.